Texas 2-Step: A new Model for YcgR::c-di-GMP Action at the Flagellar Motor

Nabin Bhattarai[1], Wangbiao Guo[2], Jonathan D Partridge[1], and Rasika M. Harshey*[1]

[1]Department of Molecular Biosciences and

LaMontagne Center for Infectious Diseases,

The University of Texas at Austin,

Austin, Texas, USA

[2]Microbial Sciences Institute & Department of Microbial Pathogenesis, Yale School of

Medicine, New Haven, Connecticut, USA

* Corresponding author: rasika@austin.utexas.edu

Abstract

YcgR is a c-di-GMP effector that inhibits both chemotaxis and swimming speed in *E. coli* and *Salmonella*. Genetic, biochemical and structural data suggest that YcgR interacts with the bidirectional flagellar rotor as well as the stator to alter rotor bias to CCW and reduce motor speed, but how both feats are achieved remain unclear. Recent cryo-EM structures showing changes in disposition of the rotor and stator units during directional changes suggested to us a mechanism by which YcgR might bring about its action. We call this the Texas 2-Step model. In the first step, YcgR interacts with a MotA subunit in the CCW conformation of the rotor where the stators are largely outside the C ring. In the second step, the rotating MotA pentamer delivers YcgR to FliG, affecting bias and speed. We provide evidence for the first step of this model, which generates testable new insights.

Importance

To date, the mechanism of YcgR action has been investigated by multiple labs using a variety of techniques, but no consensus has emerged. Some studies have favored action at the rotor, others at the stator. The complicating factor has been the involvement of four proteins - MotA, FliG, FliM, YcgR – in cross-interactions, with multiple regions in some of these proteins participating in the interaction. The availability of rotor-stator cryo-EM structures has clarified the picture, leading us to propose and test a new model that explains most, if not all the available data.

Introduction

Among the many outputs of c-di-GMP signaling, a ubiquitous one is inhibition of bacterial motility (Jenal *et al.*, 2017). The inhibitory effect on flagellar motility is well-studied in *E. coli* and *Salmonella* and is orchestrated via interaction of the c-di-GMP effector YcgR with both the flagellar rotor and stator (Boehm *et al.*, 2010, Fang & Gomelsky, 2010, Paul *et al.*, 2010, Wang *et al.*, 2018, Hou *et al.*, 2020, Liu *et al.*, 2022, Han *et al.*, 2023). In these bacteria, YcgR expression is under the control of the flagellar regulon, where a three-tiered regulatory cascade integrates various environmental cues and ensures an ordered assembly of the flagellum (Chevance & Hughes, 2008). Curiously, both YcgR and PdeH (also called YhjH), a strong phosphodiesterase that degrades c-di-GMP, are expressed in the last tier of the cascade (Ko & Park, 2000, Wang *et al.*, 2006, Frye *et al.*, 2006, Girgis *et al.*, 2007). PdeH is expected to keep c-di-GMP levels low when cells are all set to move, while YcgR is likely on guard to arrest motility if environmental conditions elevate c-di-GMP levels via the multiple diguanylate cyclases and phosphodiesterases that these bacteria encode (Hengge, 2009). Accordingly, mutation of *pdeH*, expected to elevate c-di-GMP levels, has an inhibitory effect on swimming motility in both bacteria (Ko & Park, 2000, Simm *et al.*, 2004, Frye *et al.*, 2006). A study that first demonstrated c-di-GMP-binding to the PilZ domain of YcgR, also showed that the inhibitory effect of the *pdeH* mutant was abrogated by deleting *ycgR*, establishing later that YcgR::c-di-GMP is the only effector for motility inhibition (Ryjenkov *et al.*, 2006, Nieto *et al.*, 2019).

The flagellar motors of *E. coli* and *Salmonella* consist of a bi-directional rotor and dynamic stators that engage and disengage with the rotor in a load-dependent manner (Berg, 2008, Lele *et al.*, 2013, Tipping *et al.*, 2013, Baker & O'Toole, 2017, Wadhwa *et al.*, 2021). The rotor includes the cytoplasmic C ring made of three proteins (FliG, FliM, FliN). FliG is at the top of the ring, interlaced with inner membrane MS ring protein FliF, which in turn links to the periplasmic rod, external hook and the long helical flagellar filament. The stators are

composed of pentameric MotA and dimeric MotB proteins (Deme *et al.*, 2020, Santiveri *et al.*, 2020). They are independent units that drift in the inner membrane in a “closed” ion-nonconducting form until they encounter the flagellar basal body, upon which they dock on top of FliG in the C ring and adopt an “open” ion-conducting conformation. Protons transiting through the MotAB complex cause conformational changes in MotA that power CW (clockwise) rotation of the pentameric MotA ring around a stationary MotB, thought to attach to peptidoglycan or some stationary moiety in the periplasm (Guo & Liu, 2022). Rotary MotA pushes on FliG, wherein a conserved patch of charged residues in MotA interact with compatible residues in the ‘torque helix’ of FliG, generating torque that results in the rotation of the C ring and all parts linked to it (Kojima & Blair, 2001). The C ring can accommodate ~11 stator units, but their numbers vary depending on external load. When attached to the flagellar filament (high load), *E. coli* motors spin at ~125 Hz; when the filament is absent (low load), motors rotate at 300 Hz or faster (Yuan & Berg, 2008, Berg, 2003). The default state of the bi-directional C ring is CCW (counterclockwise). The chemotaxis signal CheY~P, interacts with FliM/FliN located below FliG to elicit a large change in the C-terminal domain of FliG ($FliG_C$) where the torque helix is located, as well as producing changes at $FliG_N$, concomitantly switching the orientation of charges in the torque helix of FliG and the rotational direction of the C ring from CCW to CW (Johnson *et al.*, 2024, Singh *et al.*, 2024, Tan *et al.*, 2024). Between $FliG_C$ and $FliG_N$ is located a ‘cleft’ whose width changes from 30Å in CCW state to 40Å in the CW state. As first observed in *Borrelia burgdorferi* where the entire structure of the stator-associated rotor is visible, changes in $FliG_C$ not only change the size of the FliG ring, but also change the disposition of the stators, which move inwards in the CW state and outward in the CCW state (Chang *et al.*, 2020). Similar events at the C ring were reported in *Salmonella* (Johnson *et al.*, 2024, Singh *et al.*, 2024, Tan *et al.*, 2024), where the diameter of the upper FliG ring toggles between ~446 Å in the CW state to ~466 Å in the CCW state (Tan *et al.*, 2024). In the CW state, the rotating MotA pentamer would interact not only with $FliG_C$ but also with $FliG_N$, where charged residues similar to the torque

helix in $FliG_C$ are located (in *E. coli*, $FliG_N$ residues 26-51 are similar to $FliG_C$ residues 275-305). A genetic fusion between stators of a closely related bacterium and the torque helix in $FliG_c$ (Johnson *et al.*, 2024), as well as docking simulations (Singh *et al.*, 2024, Tan *et al.*, 2024), show that like seen in *B. burgdorferi*, stators must relocate in and out of the FliG ring (Fig. 1).

<u>The hard problem of YcgR action at the motor.</u> YcgR has been investigated for over a decade, yet its mechanism of action remains elusive. As discussed below, perhaps the overriding factor has been the interaction of both rotor (FliG, FliM) and stator (MotA) proteins with YcgR, with regions at the N- and C-termini of both FliG and YcgR participating in the interaction. The availability of rotor-stator cryo-EM structures (described above) has clarified the picture somewhat, leading us to propose and test a new model described below. To place our findings in context and better appreciate the conflicting reports in the literature, we first review and organize what is currently known about YcgR. To help the reader follow along, Fig. 2 shows the structures being discussed: C ring subunits (FliN/M/G) in the CCW and CW orientation docked with pentameric MotA (Fig. 2A) and YcgR bound to c-di-GMP (Fig. 2B). To avoid verbosity, we will refer henceforth to YcgR::ci-di-GMP simply as YcgR, unless a distinction is made.

1. <u>YcgR binds to FliG and MotA, skews rotor bias to CCW, and slows the motor</u>. Clues to the specifics of YcgR action at the motor first came from the observation that mutations in *pdeH* had a strong CCW bias (Girgis *et al.*, 2007). The skewed bias was corroborated by two studies that followed, both of which showed an interaction of YcgR with the rotor, implicating FliG (and FliM; see below) as the interacting partner(s) (Paul *et al.*, 2010, Fang & Gomelsky, 2010). Motor speeds in the *pdeH* mutant, measured by the tethered-cell assay, showed a 30% speed reduction (Paul *et al.*, 2010). YcgR interaction with both $FliG_N$ and $FliG_C$ domains was detected in two-hybrid assays, where a $FliG_N$ fragment (residues 1-115) showed a stronger interaction than a $FliG_C$ fragment (residues 173-331); both $FliG_N$ (residues 1-103) and $FliG_C$

(residues 190-296) were also recovered in pull-down assays with YcgR-His_6 (Fang & Gomelsky, 2010). Mutation of conserved residues in the known torque helix of $FliG_C$ (residues 281-289) relieved motility inhibition and weakened, but did not lose interaction with, GST-YcgR (Paul *et al.*, 2010), supporting the finding of a second binding region in FliG that interacted with YcgR (Fang & Gomelsky, 2010). Residues in YcgR that relieved motility inhibition also mapped to both $YcgR_N$ and $YcgR_C$ (Paul *et al.*, 2010), corroborated in a later study (Han *et al.*, 2023). In summary, multiple studies show that the N- and C-terminal domains of both YcgR and FliG participate in, and are required for, motility inhibition.

Interaction of YcgR with MotA was first demonstrated in a study that monitored swimming speeds as well as looked for suppressors of Δ*pdeH* extragenic to YcgR, finding several that mapped to the charged region in MotA (residues 90-98) (Boehm *et al.*, 2010) known to interact with torque helix of $FliG_C$ (Zhou *et al.*, 1998) (Fig. 2A). The suppressors had lost YcgR binding to MotA as measured by FRET between MotA-CFP and YFP-YcgR and had restored normal swimming speed. Compared to Δ*pdeH* (elevated c-di-GMP), YFP-YcgR puncta at the rotor were diminished in the WT *pdeH*$^+$ strain as well as in the suppressors; in a Δ*motA* strain, the puncta were not observed (but see stator depletion experiments of Wang et. al. 2018 described below). In *Salmonella*, YcgR-GFP puncta were visible in a WT *pdeH*$^+$ strain; they were diminished but still observed in a Δ*motA* strain (Paul *et al.*, 2010). Interaction of YcgR with a soluble cytoplasmic fragment of MotA in a 1:4 stoichiometry was later demonstrated using size exclusion chromatography (SEC) (Hou *et al.*, 2020), corroborating the findings of Boehm et al.; neither FliG nor FliMN formed an SEC-stable complex with YcgR in this study. Later FRET biosensor experiments by the same investigators showed that YcgR could interact with FliG, although the affinity was significantly lower than that of MotA (Han *et al.*, 2023).

The PilZ domain of YcgR ($YcgR_C$) binds c-di-GMP, the binding site identified to reside between $YcgR_N$ and $YcgR_C$ domains by mutagenesis (Ryjenkov *et al.*, 2006). A crystal

structure of YcgR with and without c-di-GMP, found that c-di-GMP binding caused a rearrangement of $YcgR_C$, exposing an α-helix at the very end of the C-terminus (C-tail) (Fig. 2B, green helix), and that mutations within either C-tail residues or the conserved MotA charged residues, both abrogated YcgR interaction with MotA as determined by SEC (Hou *et al.*, 2020). Mutations in conserved residues of $YcgR_N$, far from the MotA-binding C-tail α-helix, also restored motor speed despite the mutants being proficient in binding MotA (Han *et al.*, 2023), in keeping with studies of Paul et al. 2010 who found both $YcgR_N$ and $YcgR_C$ to be important for YcgR function.

In summary, YcgR associates stably with MotA and also binds both $FliG_N$ and $FliG_C$. The C-tail of $YcgR_C$ binds strongly to MotA at the region where MotA normally interacts with $FliG_C$. $YcgR_N$, which does not interact with MotA, plays an equally important, but undeciphered role in YcgR action. In WT *pdeH*$^+$ strains as well as in MotA suppressors, fluorescent fusions of YcgR, while diminished in number, are nonetheless observed at the motor.

2. <u>YcgR binds to FliM</u>. While multiple lines of evidence have established that YcgR binds FliG and MotA, significant binding of YcgR to FliM has been seen in only one study using three methods - pull downs, visualization of YcgR-GFP to the rotor, and motility assays (Paul *et al.*, 2010). Curiously, YcgR 118R→D, a mutant reported to not bind c-di-GMP nor affect motor bias and speed, as well as YcgR 147S→A, a mutant reported to bind c-di-GMP with somewhat higher affinity and inhibit motility *in vivo* better than the wild-type YcgR, were both observed to interact with FliM although not as well as with FliG (Fang & Gomelsky, 2010, Paul *et al.*, 2010, Ryjenkov *et al.*, 2006). These studies make a credible case for YcgR interacting with FliM. In pull-downs using GST-YcgR, the YcgR-interacting region of FliM mapped to a region known to interact with FliG, i.e. at the interface of FliM and FliG (Paul *et al.*, 2010).

3. <u>Two populations of YcgR: strong binding to rotor after stator depletion</u>. Evidence for two populations of YcgR comes from two studies. In a FRAP study with mEGFP-YcgR

expressed in a *pdeH* mutant, where fluorescence bleaching and its recovery at the motor were monitored using total internal reflection fluorescence (TIRF) with cells tethered to glass coverslip via a shortened flagellar filament, 36% of molecules were found to be weakly bound (exchanging), the remaining being tightly bound (non-exchanging) (Liu *et al.*, 2022). This study also determined that there was no competitive binding between YcgR and the chemotaxis signaling protein CheY~P to the motor. Evidence that the tightly bound YcgR population is at the rotor and not the stator comes from using a similar TIRF set up where the fluorescence of eGFP-YcgR at the motor was measured before and after addition NaN_3, known to deplete cellular PMF and cause stators to dissociate from the rotor; absence of a change in fluorescence intensity ± NaN_3 led to the conclusion that YcgR at the motor is bound stably mainly to the rotor (Wang *et al.*, 2018).

In summary, the TIRF studies monitoring YcgR at a motor showed strong binding to the rotor after stator depletion, very likely at FliG.

Results and Discussion

New Model for YcgR action: Texas 2-step

As described above, multiple studies have demonstrated that in a *pdeH* mutant, chromosomal levels of YcgR elicit both speed reduction and a CCW rotor bias. In a *pdeH ycgR* double mutant, where YcgR was provided on an inducible plasmid (Nieto *et al.*, 2019), rotor bias was observed to change prior to or concomitant with a decrease in motor speed. To explain these data in the context of new knowledge of the two C ring conformations (Fig. 2A), we propose the following model we call the 'Texas 2-step'. We suggest that first, $YcgR_C$ binds to MotA effectively only in the CCW state of the rotor where the stators are at the outer edge of the C ring and thus accessible for binding (Fig. 1). Next, as the $YcgR_C$-bound MotA pentamer docked on FliG begins to rotate, $YcgR_N$ is delivered to FliG. In this second step,

we can imagine two possibilities. YcgR can either straddle $FliG_C$ and MotA through its two domains, stopping rotation of the bound MotA pentamer (Movie 1), or be delivered to $FliG_N$ (Movie 2), in both cases skewing the bias to CCW and reducing speed as more FliG subunits engage with YcgR. The proposed first step of this model makes a strong prediction: this step should be proscribed in CW-locked rotors where the stators move inwards, shielding the YcgR-binding region of MotA.

A test of the first step of the model. We used two *E. coli* parent strains into which we introduced mutations to produce either a CCW or CW rotor bias as follows: Δ*cheY* - CCW, Δ*cheZ* - CW, $fliG_{\Delta PAA}$ (deletion of PAA residues 169-171) - extreme or 'locked' CW (Togashi *et al.*, 1997). MG1655-derived strains had both *pdeH* and *ycgR* deleted in the chromosome (WT**), while HCB5-derived strains had only *pdeH* deleted (WT*). YcgR was provided on an inducible plasmid as done earlier (Nieto *et al.*, 2019). Motor behavior was monitored using a bead assay, where a 0.75 μm polystyrene bead is attached to a stub of a sheared flagellar filament on bacteria fixed to a glass slide, and rotation of the bead captured by high-speed videos (see Methods); at least 15 motors were monitored for each strain, recorded continuously for 10 min after inducer addition.

Upon YcgR induction, the WT* strain showed three patterns – a complete CCW bias with a simultaneous change in speed, followed by gradual speed reduction (Fig 3A, top), complete CCW bias followed by sudden motor arrest (Fig. 3A, bottom), or no change in bias before sudden motor arrest (Fig. S1A, top). The WT** also showed these behaviors in addition to behavior reported earlier where a predominant CCW bias was followed by gradual speed reduction (Fig. S1A, bottom) (Nieto *et al.*, 2019). The Δ*cheY* strain with an initial CCW bias behaved similarly to the two WT strains in that some motors reduced speed gradually (Fig. 3B, top trace), while others stopped abruptly without an initial speed reduction (Fig. 3B, bottom trace).

The two CW-biased strains - Δ*cheZ* and FliGΔPAA - appeared largely impervious to YcgR (Fig. 3C-D). Δ*cheZ* motors were predominantly CW with an 'unstable' bias in the sense that several forays into the CCW zone were observable, but the motors were unresponsive to YcgR (Fig. 3C). When the bead size was 0.99 μm, the CW bias of Δ*cheZ* motors was even more unstable (Fig. S1B, traces before YcgR induction); upon YcgR induction, two of these motors showed a change in bias to CCW concomitant with speed reduction (Fig. S1B, top and bottom), followed by a complete CCW bias and speed reduction in one of these two motors (Fig. S1B, bottom), much like that seen the motor traces in Figure 3A (top). FliGΔPAA motors showed a stable or 'locked' CW bias, with most motors resistant to YcgR (Fig. 3D, top and bottom). However, in both WT* and WT**, ~10% of the CW-locked motors showed either a gradual decrease in speed (Fig. S1CD, top), a sudden stop (Fig. S1C, bottom) or a gradual decrease followed by a stop (Fig. S1D, bottom); thus, YcgR could access a minority of the CW-locked motors. We note that the cleft between $FliG_N$ and $FliG_C$ is larger in a CW rotor, and that a density consistent with that of YcgR has been observed in one data set from FliGΔPAA motors (Singh *et al.*, 2024).

<u>The second step</u>. Movie 1 uses Alphafold prediction of YcgR-bound MotA based on the structure of YcgR::c-di-GMP alone (Hou *et al.*, 2020), to propose that $YcgR_N$ can contact and bind $FliG_C$ as the $YcgR_C$-bound MotA pentamer rotates across FliG. However, there is a distinct possibility that YcgR changes conformation upon binding MotA, suggested by the observation that when tested with individually expressed proteins, YcgR binding to FliG is weak (Hou *et al.*, 2020, Han *et al.*, 2023), yet when stators are depleted from YcgR-bound motors, YcgR is found tightly bound to the rotor (Wang *et al.*, 2018). Thus, Movie 1 may not fully recapitulate events at the motor. Because YcgR has been shown to bind both $FliG_N$ and $FliG_C$ in pull-down and two-hybrid assays (Fang & Gomelsky, 2010), we can imagine a scenario where $YcgR_N$ binds $FliG_N$ rather than $FliG_C$, releasing $YcgR_C$ from MotA in the process (Movie 2). If YcgR were to be located at $FliG_N$, it could enable an initial CCW bias

without immediately reducing speed (Fig. 3A and S1A, bottom). More experiments will be needed to distinguish between these possibilities.

A summary of the motors tracked in this study is shown in Fig. S2. While the data in Fig. 3 were generated with 0.75μm beads, we also monitored WT** motors with smaller (0.45μm) and larger (0.99μm) beads, expected to exert lower and higher loads on the motor, respectively. A noticeable trend was that upon YcgR induction, more motors stopped with smaller beads compared to larger ones. Motor torque is expected to vary with bead size, with fewer stators engaged at the rotor when the bead size is small and vice versa, explaining the trend with different bead sizes.

Other insights and caveats. 1. Motor behavior from chromosomal levels of YcgR (Fig. 4B; *pdeH*) as well as from plasmid-induced levels (Fig. S1B; *pdeH ycgR cheZ)* shows that despite speed reduction and CCW bias, these motors still switch. This would imply that YcgR-occupied FliG subunits do not hinder unoccupied ones from switching, in contrast to the uniform configuration of all FliG subunits seen in cryo-EM images of CCW and CW rotors (Johnson *et al.*, 2024, Singh *et al.*, 2024, Tan *et al.*, 2024).

2. The resistance of MotA suppressor mutants to YcgR (Boehm *et al.*, 2010), is not inconsistent with Step 1 of our model where access to the torque-generating region of FliG is *obligatorily* through MotA. Our deduction that MotA-binding induces a conformational change in YcgR necessary for stable binding to FliG (see 'The second step') should be testable.

3. We obtained the YcgR-resistant MotA suppressors G93E, G93R, G93V and S96L described by Boehm *et al*. and confirmed their phenotype using migration in soft agar (Fig. 4A). Bead assays with several of the suppressors showed that they had restored normal motor bias but had lower speeds (50-70 Hz) compared to WT (80Hz) (Fig. 4B,C). These lower speeds were intrinsic to the suppressor mutation because they were maintained even when the native copy of *ycgR* was deleted (Fig. 4B, only the S96L motor in Δ*ycgR* shown).

The pattern of charged residues important for interaction with MotA in the torque helix in $FliG_C$ is also seen in the $FliG_N$ α-helix, consistent with MotA interaction that must occur at both $FliG_N$ and $FliG_C$ when the stators occupy both in the CW state (Johnson *et al.*, 2024). Given the multiple lines of evidence showing interaction of YcgR with FliG residues in both $FliG_C$ and $FliG_N$, why were suppressor mutations not recovered in FliG in the Boehm et. al. study? One explanation is that if YcgR can bind to both $FliG_N$ and $FliG_C$, the likelihood of mutating both would be low. An alternative explanation is that these mutations affected motor bias and therefore were not detected in motility assays that required the mutants to be chemotaxis-proficient and migrate out in a soft-agar plate (Fig. 4A).

4. It is formally possible that the observed interaction of YcgR with both $FliG_N$ and $FliG_C$ in pull-down and two-hybrid assays is due to the homologies within these regions and have no bearing on the proposed alternate event at the second step (Movie 2).

5. In contrast to *E. coli* YcgR, the YcgR homolog MotI/DgrA of *Bacillus subtilis* does not affect motor bias, acting instead as a molecular clutch by binding to and disengaging MotA from the C ring to arrest rotation (Subramanian *et al.*, 2017). The advantages of evolving different strategies to control motor behavior by two related proteins is conjectural, but they nonetheless converge under some conditions: subinhibitory concentrations of MotI do what YcgR does – reduce swimming speed – and high concentrations of YcgR do what MotI does – stop the motor.

Acknowledgments

This model was inspired by the first published images of the *Borrelia* motor from Jun Liu's lab showing differences in stator disposition at the rotor; we thank him for discussions. We also thank Urs Jenal for MotA suppressors and Birgit Scharf for *E. coli* strain HCB5. This

work was supported by NIH grant GM118085 to RMH.

Methods

Strains and growth conditions

Strains and plasmids used in this study are listed in **Table S1**. Bacterial cultures were grown in Lennox broth (LB) base (20 g/liter) (Fisher BioReagents). For motility assays in soft agar, 8 µl of an exponential-phase culture (optical density at 600 nm [OD_{600}], ~0.6) was inoculated onto plates made with 0.3% Bacto agar (Difco) and incubated at 30°C. All plate images shown are representative of three biological replicates, each in triplicate. Where required, the following antibiotics were used: ampicillin (100 µg/ml), chloramphenicol (20 µg/ml), and kanamycin (50 µg/ml). For inducible plasmids, 50uM IPTG (isopropyl-β-d-thiogalactopyranoside) and 0.2% L-arabinose were used.

Genetic manipulation

The WT parent strains for *E. coli* were MG1655 and HCB5. Mutant strains were constructed by inserting a kanamycin resistance cassette (KAN) into the designated gene as previously described (Datsenko & Wanner, 2000) or sourced from the Keio collection (Baba *et al.*, 2006). Mutations were transferred to fresh backgrounds by phage P1 (P1 Cm) transduction. Excision of the inserted KAN cassettes was achieved by expression of the FLP recombinase encoded by pCP20 (Datsenko & Wanner, 2000).The resulting strains were confirmed by DNA sequencing. A 3 amino acid deletion of residues 169-171 (PAA) in FliG was introduced using the CRMAGE protocol (Ronda *et al.*, 2016), which leverages CRISPR-Cas9 technology as follows: A cocktail of 3 primer pairs for making guide RNAs (gRNA) targeting *fliG* were cloned into pMAZ-SK plasmid via Golden Gate assembly; gRNAs are expressed with anhydrotetracycline (aTetracycline). These constructs were introduced along with repair oligonucleotides into NBN28 containing pMA7CR_2.0, which expresses the λ Red β-protein and the CRISPR/Cas9 protein upon induction with L-arabinose. The insertion was confirmed

by PCR amplification followed sequencing. All the primers and oligonucleotides used are listed in Table S2.

Measurement of motor dynamics using bead assay

The bead assay was conducted as described in the previous work (Nieto *et al.*, 2019, Partridge *et al.*, 2015). *E. coli fliC* deletion strains (containing additional chromosomal mutations) were complemented with pFD313 expressing the 'sticky' FliC variant (Ryu *et al.*, 2000), and pSEVA224 expressing YcgR. First, cells were passed through two syringes connected by a 7” polyethylene capillary to shear the flagella. A 40 µL cell suspension was then added to a poly-l-lysine-coated cover slip, incubated for 10 minutes, and rinsed with motility buffer to remove unattached cells (Partridge & Harshey, 2020). A 40 µL solution of polystyrene beads (1:50 dilution) was added and left for 10 minutes before excess beads were washed away, prior to introducing IPTG for inducing YgcR expression. Bead rotations were captured at 1,000 frames/s using a CCD camera (ICL-B0620M-KC0; Imperx, Boca Raton, FL). Videos were processed using custom analytical programs within LabVIEW 2012 as described before (Nieto *et al.*, 2019).

Animation

Animation illustrating YcgR-mediated regulation of the stator–C-ring complex. was created using ChimeraX 1.9 and assembled in Keynote. Structural models used include YcgR (PDB: 5Y6F), C-ring in CW and CCW conformations (PDB: 8UMX and 8UMD, respectively), and MotA (PDB: 6YKM).

Main Figures

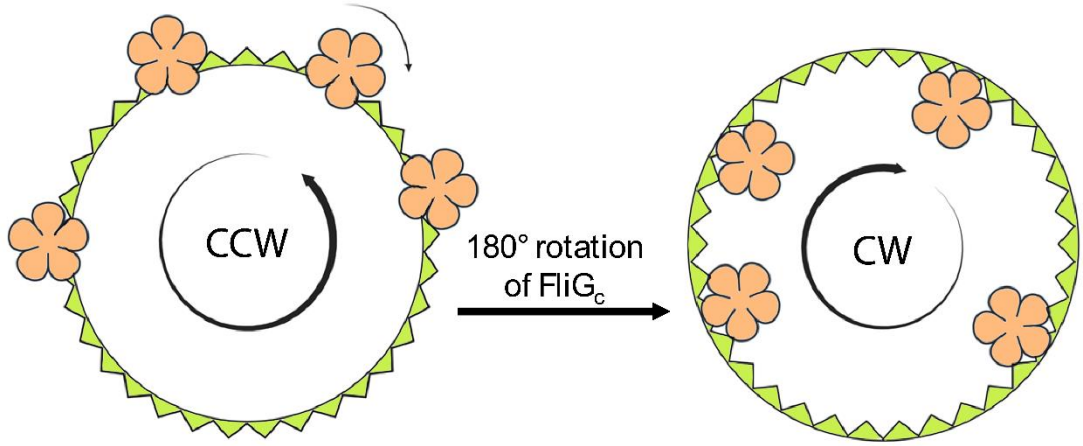

Figure 1. **Rotational switching of the C ring.** The binding of CheY~P at the bottom the C ring (not shown) leads to a conformational change of FliG$_C$ at the top of the ring (green triangles), inducing a movement of the stators (orange pentamer) from outside the FliG ring (left) to inside (right), concomitantly switching rotation direction from CCW to CW.

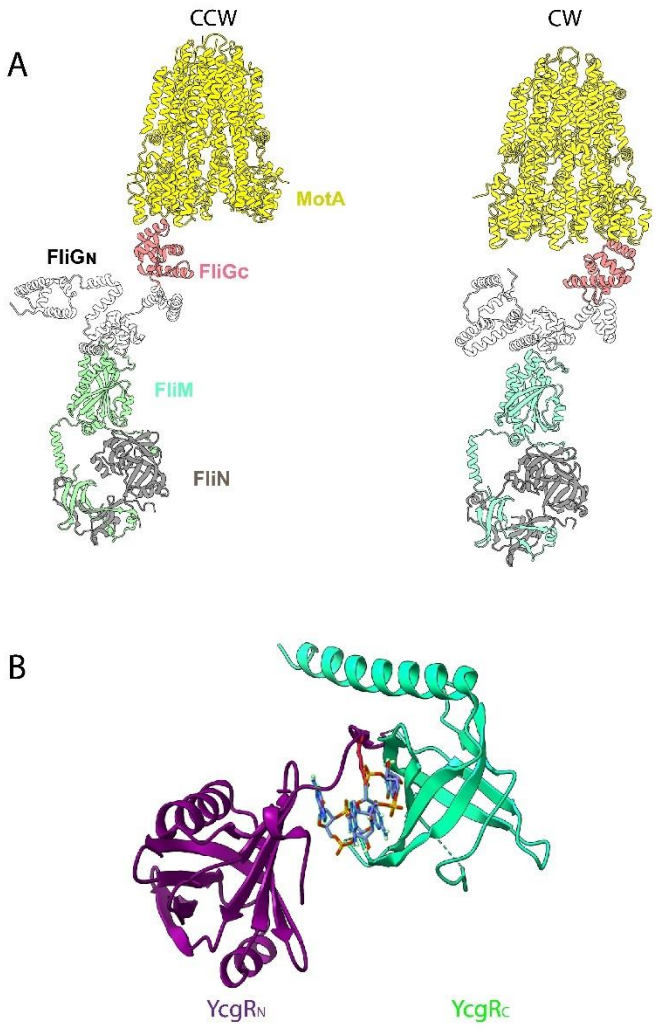

Figure 2. **Structures of C ring subunits, MotA and YcgR**. A) Pentameric MotA (PDB: 6YKM) docked on the torque-helix of a single $FliG_C$ subunit of the C ring (FliG, FliM, FliN) in its CCW and CW orientations (PDB: 8UMX and 8UMD, respectively). B) Structure of YcgR with bound c-di-GMP (PDB: 5Y6F). See text for details.

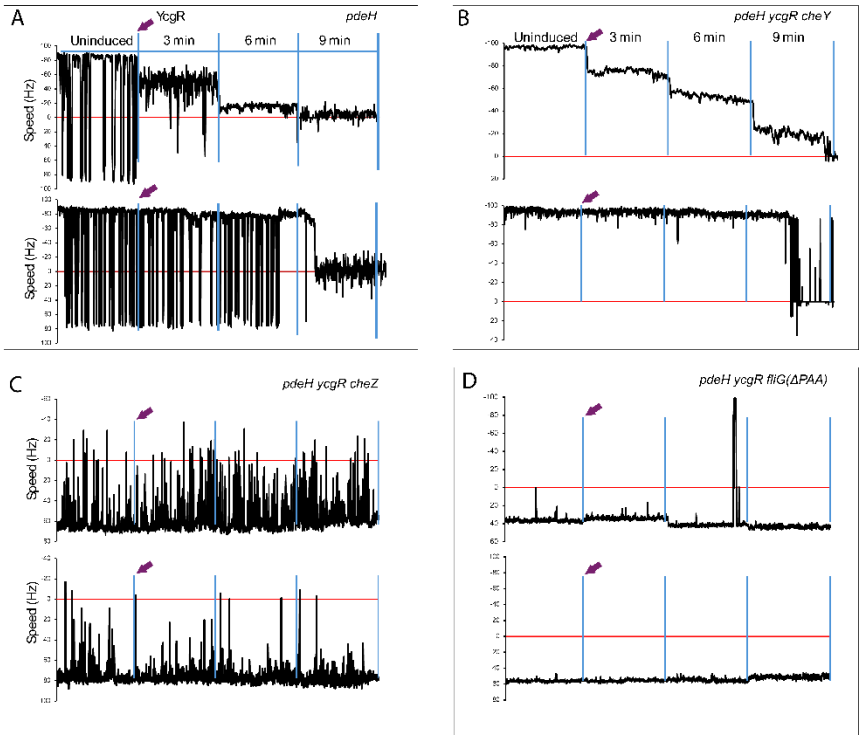

Figure 3. Response of WT, CCW and CW motors to YcgR. A) Representative motors from WT* HCB5 strain with YcgR supplied from an IPTG-inducible low copy plasmid pSEVA224, monitored by recording the motion of 0.75 μm polystyrene beads attached to filament stubs (see Methods). After IPTG addition (arrow), 60-second representative segments from each consecutive 3-minute recording interval are shown. Counterclockwise (CCW or -) and clockwise (CW or +) speeds in Hz are shown on the Y-axis. The profiles are representative of 15 individual motors tracked (see Fig. S2). B) As in A, except the strain is WT** MG1655 and has *cheY* deleted. C) As in B, except *cheZ* is deleted. D) As in B, except *fliG* was deleted for nucleotides encoding PAA at residues 169-171 in FliG.

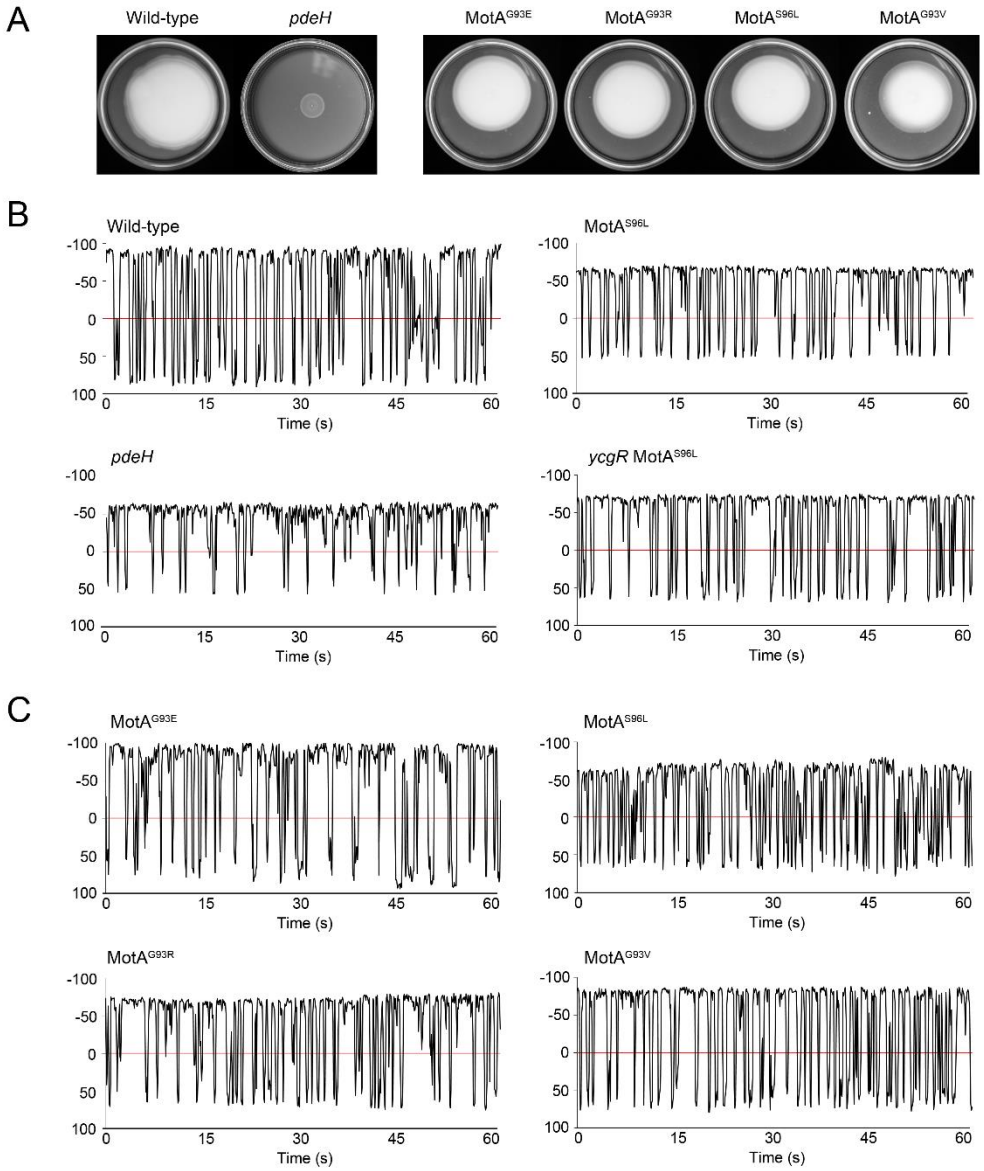

Figure 4. Swimming and motor behavior of MotA suppressors. A) Motility assays were conducted in soft agar (see Methods). Left panel, motility is inhibited in a *pdeH* mutant (WT, MG1655; *pdeH,* AB607). Right panel, four MotA suppressors that overcame the motility defect of the *pdeH* mutant, described by Boehm et al. (see Table S1 for strain numbers). B) Bead assays in WT and indicated $MotA^{S96L}$ suppressor (AB1577) in which *ycgR* was deleted (JP1501). C) Bead assays in four MotA suppressor strains. The WT strain is MG1655 for all motors, monitored with 0.75 μm polystyrene beads. Representative traces of 15 motors each are shown.

Supplementary Figures and Movies

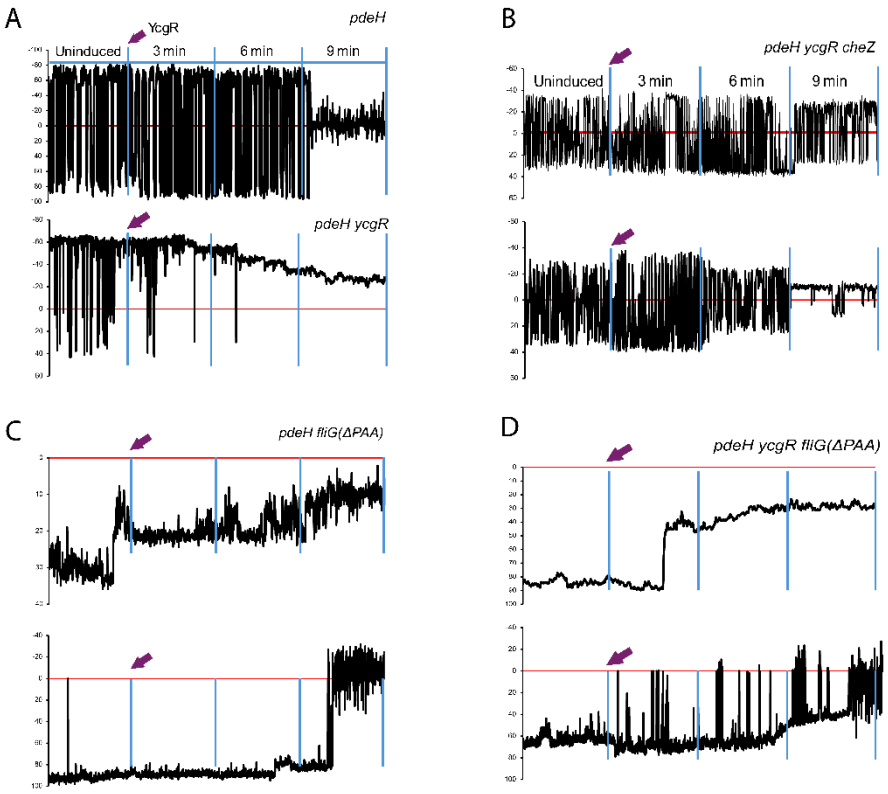

Figure S1. Behavior of CW motors and Summary of motor data. Each panel shows traces of two representative motors in strains whose genotype is indicated on the upper right; see Fig. S2 for summary of all motors. Bead size is 0.75 μm in all panels except B, where it is 0.99 μm. Other descriptions as in Fig. 3A.

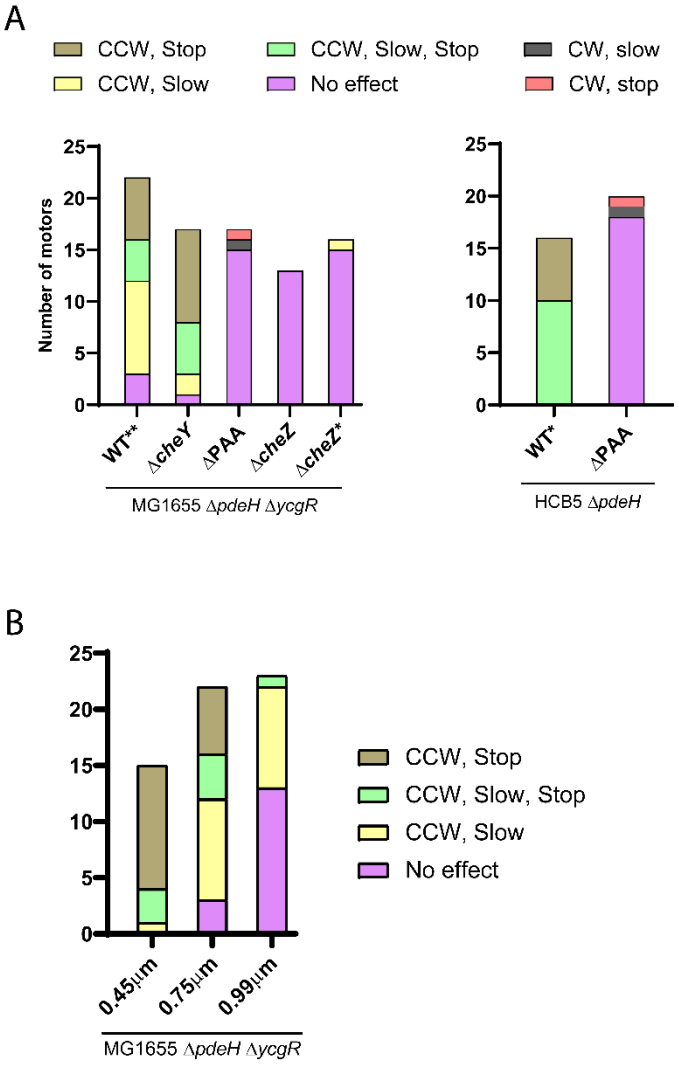

Figure S2. Summary of all motor traces. A) Bead size is 0.75 μm for all graphs except the one marked with an * where the bead size was 0'99 μm. B) Data were obtained for with three bead sizes WT**.

Movie 1. YcgR interaction with CCW stator–C ring complex, straddling MotA and $FliG_C$. The animation was created using ChimeraX 1.9 and assembled in Keynote. Structural models used include YcgR (PDB: 5Y6F), CCW C-ring (PDB: 8UMD), and MotA (PDB: 6YKM).

Movie 2. YcgR interaction with CCW stator–C ring complex at $FliG_N$. Structural models as in Movie 1. Residue information for YcgR, MotA and FliG provided directly on the image.

References

Baba, T., Ara, T., Hasegawa, M., Takai, Y., Okumura, Y., Baba, M., Datsenko, K.A., Tomita, M., Wanner, B.L., and Mori, H. (2006) Construction of *Escherichia coli* K-12 in-frame, single-gene knockout mutants: the Keio collection. *Mol Syst Biol* **2**: 2006.0008.

Baker, A.E., and O'Toole, G.A. (2017) Bacteria, Rev Your Engines: Stator Dynamics Regulate Flagellar Motility. *J Bacteriol* **199**.

Berg, H.C. (2003) The rotary motor of bacterial flagella. *Annu Rev Biochem* **72**: 19-54.

Berg, H.C. (2008) Bacterial flagellar motor. *Current biology : CB* **18**: R689-691.

Boehm, A., Kaiser, M., Li, H., Spangler, C., Kasper, C.A., Ackermann, M., Kaever, V., Sourjik, V., Roth, V., and Jenal, U. (2010) Second messenger-mediated adjustment of bacterial swimming velocity. *Cell* **141**: 107-116.

Chang, Y., Zhang, K., Carroll, B.L., Zhao, X., Charon, N.W., Norris, S.J., Motaleb, M.A., Li, C., and Liu, J. (2020) Molecular mechanism for rotational switching of the bacterial flagellar motor. *Nat Struct Mol Biol* **27**: 1041-1047.

Chevance, F.F., and Hughes, K.T. (2008) Coordinating assembly of a bacterial macromolecular machine. *Nature Rev Microbiol* **6**: 455-465.

Datsenko, K.A., and Wanner, B.L. (2000) One-step inactivation of chromosomal genes in *Escherichia coli* K-12 using PCR products. *Proc Natl Acad Sci U S A* **97**: 6640-6645.

Deme, J.C., Johnson, S., Vickery, O., Aron, A., Monkhouse, H., Griffiths, T., James, R.H., Berks, B.C., Coulton, J.W., Stansfeld, P.J., and Lea, S.M. (2020) Structures of the stator complex that drives rotation of the bacterial flagellum. *Nat Microbiol* **5**: 1553-1564.

Fang, X., and Gomelsky, M. (2010) A post-translational, c-di-GMP-dependent mechanism regulating flagellar motility. *Mol Microbiol* **76**: 1295-1305.

Frye, J., Karlinsey, J.E., Felise, H.R., Marzolf, B., Dowidar, N., McClelland, M., and Hughes, K.T. (2006) Identification of new flagellar genes of *Salmonella enterica* serovar Typhimurium. *J Bacteriol* **188**: 2233-2243.

Girgis, H.S., Liu, Y., Ryu, W.S., and Tavazoie, S. (2007) A comprehensive genetic characterization of bacterial motility. *PLoS Genet* **3**: 1644-1660.

Guo, S., and Liu, J. (2022) The Bacterial Flagellar Motor: Insights Into Torque Generation, Rotational Switching, and Mechanosensing. *Front Microbiol* **13**: 911114.

Han, Q., Wang, S.F., Qian, X.X., Guo, L., Shi, Y.F., He, R., Yuan, J.H., Hou, Y.J., and Li, D.F. (2023) Flagellar brake protein YcgR interacts with motor proteins MotA and FliG to regulate the flagellar rotation speed and direction. *Front Microbiol* **14**: 1159974.

Hengge, R. (2009) Principles of c-di-GMP signalling in bacteria. *Nat Rev Microbiol* **7**: 263-273.

Hou, Y.J., Yang, W.S., Hong, Y., Zhang, Y., Wang, D.C., and Li, D.F. (2020) Structural insights into the mechanism of c-di-GMP?bound YcgR regulating flagellar motility in Escherichia coli. *Journal of Biological Chemistry* **295**: 808-821.

Jenal, U., Reinders, A., and Lori, C. (2017) Cyclic di-GMP: second messenger extraordinaire. *Nat Rev Microbiol* **15**: 271-284.

Johnson, S., Deme, J.C., Furlong, E.J., Caesar, J.J.E., Chevance, F.F.V., Hughes, K.T., and Lea, S.M. (2024) Structural basis of directional switching by the bacterial flagellum. *Nat Microbiol* **9**: 1282-1292.

Ko, M., and Park, C. (2000) Two novel flagellar components and H-NS are involved in the motor function of *Escherichia coli*. *J Mol Biol* **303**: 371-382.

Kojima, S., and Blair, D.F. (2001) Conformational change in the stator of the bacterial flagellar motor. *Biochemistry* **40**: 13041-13050.

Lele, P.P., Hosu, B.G., and Berg, H.C. (2013) Dynamics of mechanosensing in the bacterial flagellar motor. *Proc Natl Acad Sci U S A* **110**: 11839-11844.

Liu, X., Zhang, C., Zhang, R., and Yuan, J. (2022) The Effect of the Second Messenger c-di-GMP on Bacterial Chemotaxis in Escherichia coli. *Appl Environ Microbiol* **88**: e0037322.

Nieto, V., Partridge, J.D., Severin, G.B., Lai, R.Z., Waters, C.M., Parkinson, J.S., and Harshey, R.M. (2019) Under Elevated c-di-GMP in Escherichia coli, YcgR Alters Flagellar Motor Bias and Speed Sequentially, with Additional Negative Control of the Flagellar Regulon via the Adaptor Protein RssB. *J Bacteriol* **202**.

Partridge, J.D., and Harshey, R.M. (2020) Investigating Flagella-Driven Motility in Escherichia coli by Applying Three Established Techniques in a Series. *J Vis Exp*.

Partridge, J.D., Nieto, V., and Harshey, R.M. (2015) A new player at the flagellar motor: FliL controls both motor output and bias. *MBio* **6**: e02367.

Paul, K., Brunstetter, D., Titen, S., and Blair, D.F. (2011) A molecular mechanism of direction switching in the flagellar motor of Escherichia coli. *Proc Natl Acad Sci U S A* **108**: 17171-17176.

Paul, K., Nieto, V., Carlquist, W.C., Blair, D.F., and Harshey, R.M. (2010) The c-di-GMP binding protein YcgR controls flagellar motor direction and speed to affect chemotaxis by a "backstop brake" mechanism. *Molecular cell* **38**: 128-139.

Ronda, C., Pedersen, L.E., Sommer, M.O., and Nielsen, A.T. (2016) CRMAGE: CRISPR Optimized MAGE Recombineering. *Sci Rep* **6**: 19452.

Ryjenkov, D.A., Simm, R., Romling, U., and Gomelsky, M. (2006) The PilZ domain is a receptor for the second messenger c-di-GMP: the PilZ domain protein YcgR controls motility in enterobacteria. *J Biol Chem* **281**: 30310-30314.

Ryu, W.S., Berry, R.M., and Berg, H.C. (2000) Torque-generating units of the flagellar motor of *Escherichia coli* have a high duty ratio. *Nature* **403**: 444-447.

Santiveri, M., Roa-Eguiara, A., Kuhne, C., Wadhwa, N., Hu, H., Berg, H.C., Erhardt, M., and Taylor, N.M.I. (2020) Structure and Function of Stator Units of the Bacterial Flagellar Motor. *Cell* **183**: 244-257 e216.

Simm, R., Morr, M., Kader, A., Nimtz, M., and Romling, U. (2004) GGDEF and EAL domains inversely regulate cyclic di-GMP levels and transition from sessility to motility. *Mol Microbiol* **53**: 1123-1134.

Singh, P.K., Sharma, P., Afanzar, O., Goldfarb, M.H., Maklashina, E., Eisenbach, M., Cecchini, G., and

399 Iverson, T.M. (2024) CryoEM structures reveal how the bacterial flagellum rotates and
400 switches direction. *Nat Microbiol* **9**: 1271-1281.
401 Subramanian, S., Gao, X., Dann, C.E., 3rd, and Kearns, D.B. (2017) MotI (DgrA) acts as a molecular
402 clutch on the flagellar stator protein MotA in Bacillus subtilis. *Proc Natl Acad Sci U S A*
403 **114**: 13537-13542.
404 Tan, J., Zhang, L., Zhou, X., Han, S., Zhou, Y., and Zhu, Y. (2024) Structural basis of the bacterial
405 flagellar motor rotational switching. *Cell Res* **34**: 788-801.
406 Tipping, M.J., Delalez, N.J., Lim, R., Berry, R.M., and Armitage, J.P. (2013) Load-dependent assembly
407 of the bacterial flagellar motor. *MBio* **4**.
408 Togashi, F., Yamaguchi, S., Kihara, M., Aizawa, S.I., and Macnab, R.M. (1997) An extreme clockwise
409 switch bias mutation in fliG of Salmonella typhimurium and its suppression by slow-motile
410 mutations in motA and motB. *J Bacteriol* **179**: 2994-3003.
411 Wadhwa, N., Tu, Y., and Berg, H.C. (2021) Mechanosensitive remodeling of the bacterial flagellar
412 motor is independent of direction of rotation. *Proc Natl Acad Sci U S A* **118**.
413 Wang, Q., Mariconda, S., Suzuki, A., McClelland, M., and Harshey, R.M. (2006) Uncovering a large
414 set of genes that affect surface motility in *Salmonella enterica* serovar Typhimurium. *J*
415 *Bacteriol* **188**: 7981-7984.
416 Wang, R., Wang, F., He, R., Zhang, R., and Yuan, J. (2018) The Second Messenger c-di-GMP Adjusts
417 Motility and Promotes Surface Aggregation of Bacteria. *Biophys J* **115**: 2242-2249.
418 Yuan, J., and Berg, H.C. (2008) Resurrection of the flagellar rotary motor near zero load. *Proc Natl*
419 *Acad Sci U S A* **105**: 1182-1185.
420 Zhou, J., Lloyd, S.A., and Blair, D.F. (1998) Electrostatic interactions between rotor and stator in the
421 bacterial flagellar motor. *Proc Natl Acad Sci U S A* **95**: 6436-6441.

422